Beam Performance

Developments and Upgrades of Storage Ring

Machine Tuning for Lower Emittance Optics of SPring-8 Storage Ring

To provide higher brilliance and flux density for the hard X-ray region than those of the present, a new optics of the SPring-8 storage ring has been examined. The design emittance of the new optics is reduced from the present emittance of 3.49 to 2.41 nm·rad at 8 GeV (Table 1). It is predicted by SPECTRA [1] that the new optics can provide 1.5 times higher brilliance and 1.25 times higher flux density for 10 keV photons with the SPring-8 standard undulator than those of the present. It is noted that, in the new optics, magnetic positions and polarities are fixed and magnetic fields are optimized within the specifications, so that the shutdown time is not required for switching from the present optics to the new one.

The machine tuning processes for the new optics, such as increase in the injection efficiency and optimization of the bump orbit for the top-up injection, have been carried out during the machine study run. It was confirmed that the top-up injection efficiency and beam lifetime of the new optics are sufficient for adopting the user operation.

The emittance was estimated by measuring the electron beam size using the X-ray beam profile monitor, and by using the lattice functions estimated from the response matrix analysis. The resulting value of the horizontal emittance shows good agreement with the design. The ratio of the vertical emittance to the horizontal emittance of the new optics is about 0.55%, which is almost the same as the present.

The test run of the new optics was demonstrated on Jan. 26, 2013 to check the photon beam performance at some beamlines. The increase in the partial flux (~10%), the increment of the brilliance (25%) and the decrease in the photon beam size at the front-end slit (10%) were observed at insertion device beamlines. After checking the photon beam performance at all beamlines, the new optics will be released to user operation from May 2013.

Table 1. Main parameters of present optics and new optics.

	Present Optics	New Optics
Beam energy	8 GeV	8 GeV
Natural emittance	3.49 nm·rad	2.41 nm·rad
Energy spread σ_E/E	0.11%	0.11%
Tune (Q_x, Q_y)	(40.14, 19.35)	(41.14, 19.35)
Natural chromaticity (ξ_x, ξ_y)	(−88, −42)	(−117, −47)
Effective emittance @ ID center	3.77 nm·rad	2.79 nm·rad
Lattice function (β_x, β_y, D) @ ID center	(22.5 m, 5.6 m, 0.11 m)	(31.2 m, 5.0 m, 0.15 m)

Improvement of Coupling Correction

The vertical beam spread, or the emittance coupling, is one of the most important parameters for the high brilliance light source storage ring. By the precise alignment of the magnets and the proper COD correction, at the commissioning phase of the SPring-8 storage ring, we succeeded in achieving the very small coupling, of ~0.2% without correction. However, the coupling had grown large over the years; thus, at present, we have corrected it and recovered the initial performance.

Recently, although the coupling has been corrected, it has become noticeable that the vertical beam spread becomes large in the magnet array gaps of some insertion devices (ID's) closed. For example, Fig. 1 shows the trend of the vertical beam size measured by the visible light interferometer in the beamline tuning time with the ID10 gap, which implies the clear effect of the ID magnetic field on the coupling. To correct the coupling induced by the ID10, we tune the skew quadrupole magnets, sk_9_3 and sk_10_2, close to the ID. The tuning was done at 10:00 on October 1, whose process is shown in Fig. 2. By adjusting the skew quadrupole magnets, we reduced the vertical beam size from 26 to 23 μm, which is the size with all ID's gaps fully open. For the purpose of independently changing the ID gap without any effect on the user beam operation, we plan to prepare the software for adjusting the strength of the skew quadrupole magnets automatically.

The vertical dispersion, which does not exist in the design and is generated by means of an error

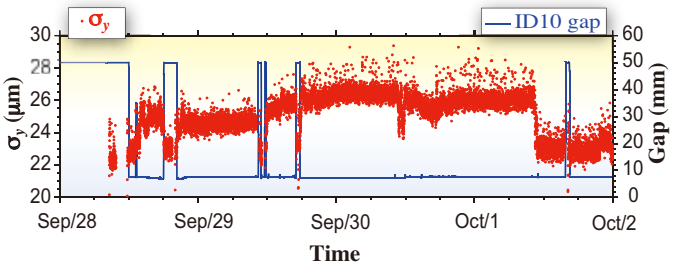

Fig. 1. Trend of vertical beam size and magnet array gap of ID10 during beamline tuning time.

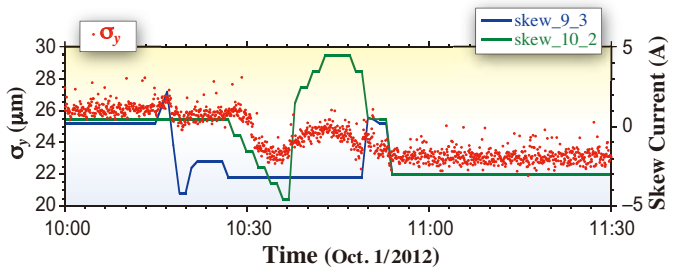

Fig. 2. Vertical beam size and currents of power supplies of skew quadrupole magnets.

magnetic field, also gives rise to the vertical beam spread, and thus is corrected as well as the coupling. To improve the vertical dispersion correction, we replace some of the skew quadrupole magnets with stronger ones and rearrange the removed ones at different locations. Figure 3 shows the vertical dispersions before and after the correction. The r.m.s. vertical dispersions are 5.01 and 0.87 mm. Before introducing the stronger skew quadrupole magnet, we can never reduce the r.m.s. vertical dispersion to sub-millimeter scale.

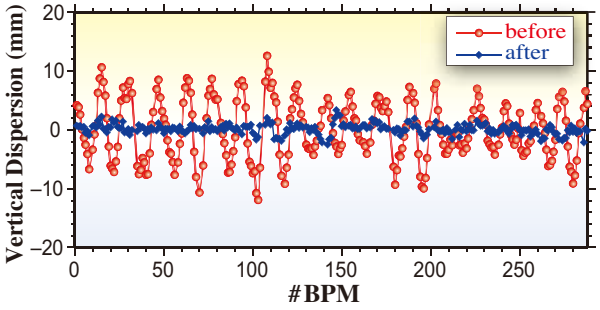

Fig. 3. Vertical dispersion before and after correction.

Design of Low-Vertical Beta Straight Section for Installing Cryoundulator

In one of the normal straight sections of the storage ring, a 1.5-m-long cryoundulator with a short period of 15 mm was installed in March 2013 and beam tests are planned to examine its performance. This cryoundulator is of the in-vacuum type and the minimum gap can be set to as small as 3 mm. At present, such a small gap value is allowed only in machine studies and not acceptable in user time due to the degradation of the beam injection efficiency and lifetime. For the present storage ring optics, the vertical betatron function takes a value of 5.6 m at the center of the normal straight section, and the minimum gap is limited to 5.6 mm to maintain stable top-up operation. To realize a gap of about 3 mm in user time, we need to modify the lattice locally to lower the vertical betatron function at this point to 1.2 m.

Figure 4 shows a design of a new lattice having a low-vertical beta straight section. The vertical betatron function will be lowered from 5.6 to 1.2 m, and this allows us to close the gap of the cryoundulator down to 3 mm. In this design of a new lattice, two families of quadrupole magnets are added to control the betatron functions at the center of the normal straight section, and the cabling of power supplies of adjacent three families of existing quadrupole magnets is changed so that they can be excited independently to fulfill matching conditions. The betatron tunes of the ring are then adjusted globally. Since the lattice functions in the rest of the ring and the emittance are unchanged, the performance of other beamlines will not be affected by this local lattice modification.

From the viewpoint of accelerator operation, however, the dynamic stability of the electron beam becomes slightly worse (the dynamic aperture shrinks by about 10 to 20%), since the symmetry of the lattice for the whole ring is broken and harmful resonances are excited. To recover the dynamic aperture and maintain the operational performance of the ring as high as possible, optimization of sextupole strengths will be carried out.

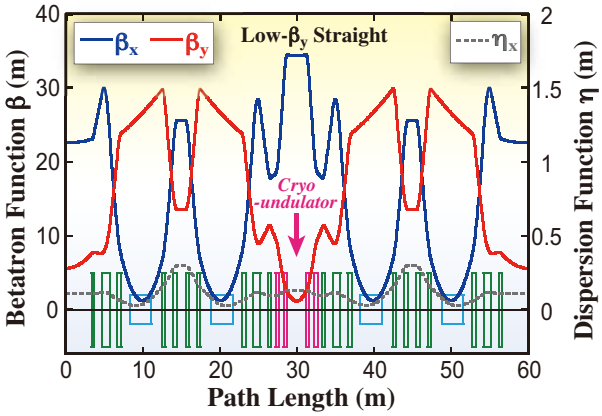

Fig. 4. Lattice functions in modified normal straight section. Also shown in the figure is the magnet arrangement (blue: bending magnets, green: quadrupole magnets, pink: quadrupole doublets to be added).

Development of Bunch-by-Bunch Feedback System

The filling mode of the storage ring named "H-mode", the hybrid filling with a 5 mA/bunch singlet and a 95 mA bunch-train of 11/29-filling with a low

bunch current of 0.1 mA/bunch, was added to the list of the user operation filling mode and was successfully put to user operation in December 2012. This mode fulfills the requests of the users of high-current isolated singlet bunch and those of high average current. The successful suppression of the beam instabilities by the SPring-8 bunch-by-bunch feedback (BBF) system is the key for this filling.

In such filling, the strong single-bunch instability of the high-current singlet and the multi-bunch instability of the bunch train, both in the horizontal and vertical betatron oscillations, have to be suppressed simultaneously by the BBF system. The BBF detects the bunch position with the beam position monitor (BPM) signal and drives the kicker to dump the oscillations. However, the BPM signal is proportional to the bunch current and to the position; hence, the BPM signal of the high-current singlet is too big for the BBF, the gain of which was tuned to the low bunch current of the bunch train. To overcome this problem, the bunch-current-sensitive fast attenuator [2] was developed to attenuate the BPM signal level of the high bunch current as shown in Fig. 5. Also, the high-efficiency horizontal kicker was installed to increase the controllable amplitude range to cover the large oscillation excited at injection.

Several attempts to increase the bunch current from 5 to 10 mA/bunch by suppressing the strong single-bunch beam instabilities are in progress, including the installation of the vertical feedback loop dedicated to the high-current singlet bunches for more flexible tuning than the fast attenuator, and the development of the new digital feedback processor. The new digital feedback processor under development can strengthen the feedback system, to update the devices for the FPGA, ADC and DAC, and to simplify the current system by merging the function of the feedback processor and the fast attenuator. In the fiscal year 2012, the hardware of the new processor composed of a brand-new Xilinx Virtex-7 FPGA board and 508 MS/s ADC/DAC boards was developed. The development of the FPGA program for the feedback operation and the PC program for the control of the FPGA board from PC through Ethernet is scheduled in the fiscal year 2013. The new feedback processor also has the capability to perform the planned new feedback schemes with which the single bunch current is intended to be raised to 10 mA/bunch from 5mA/bunch.

At the low-energy high-current operation of the SPring-8 storage ring, longitudinal multi-bunch instability driven by high-order modes of the acceleration cavities was observed, and it degraded the beam quality. To suppress this instability, the longitudinal energy kicker (Fig. 6) based on the new concept [4] developed in SPring-8 was fabricated and installed in the storage ring. This new type of kicker has several times higher shunt impedance/length than the widely used overloaded cavity-type kicker. Also, the components of the longitudinal feedback system were prepared for the feedback operation scheduled in the fiscal year 2013.

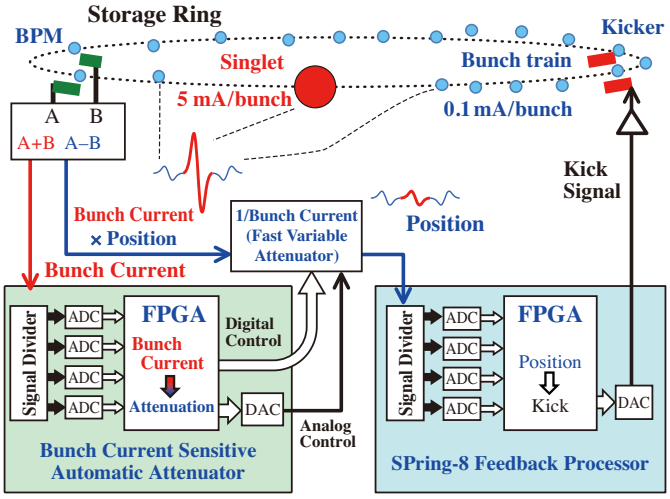

Fig. 5. Bunch current sensitive automatic attenuator (left) and feedback processor (right) for BBF for hybrid filling with high bunch current singlet and low bunch current bunch train.

Fig. 6. New high efficiency longitudinal energy kicker (3 kicker cells inside).

Development of Turn-by-Turn Beam Profile Monitor

The turn-by-turn beam profile monitor (TTPM) [4] observing monochromatic photon beam profiles of the ID has been developed. It enables us to observe fast phenomena, such as oscillations of the stored beam at top-up injections, blowups of transverse size and energy spread of a high-current single bunch caused by beam instabilities. The experimental setup of the TTPM is shown in Fig. 7. It consists of a

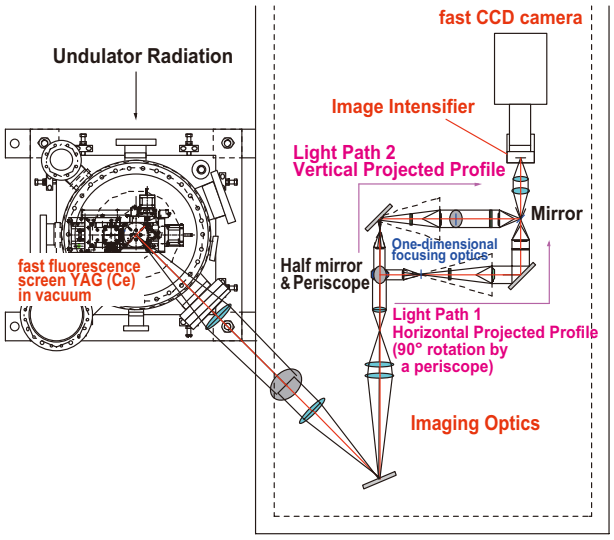

Fig. 7. Experimental setup of turn-by-turn beam profile monitor (TTPM) developed at diagnostics beamline II.

YAG (Ce) screen with decay time of several tens of nanoseconds, imaging optics and a fast CCD camera with an image intensifier (I.I.). The imaging optics of the TTPM transforms the 2D beam profile on the YAG (Ce) screen to the two line profiles projected on the horizontal and vertical axes. The fast gate by the microchannel plates (MCPs) of the I.I. selects the light from specific bunches out of all the stored bunches. The kinetics readout mode of the fast CCD camera (Roper Scientific: ProEM 512B) enables measurements with high repetition rates.

In Fig. 8, we show an example of angular oscillation of the photon beam axis of the ID observed with the TTPM at the top-up beam injection in user time. For injection, four bump magnets are excited by four individual pulsed power supplies to generate a pulsed bump orbit. A residual kick caused by the non-similarity of the temporal shape of the magnetic fields of the four pulsed magnets could excite a horizontal oscillation of the stored beam. Efforts have been made by tuning the fields of the four bump magnets to reduce the residual kick and by applying a counter kick of a fast correction magnet to the residual kick [5,6]. Although the residual kick at the temporal peak of the bump magnetic fields has been successfully suppressed, there still remains a significant kick to the stored beam at the rising part of the fields. Figure 8 shows the profiles of the photon beam of the ID obtained every 5 turns by using the kinetics readout mode of the fast CCD camera, by selecting with the I.I. those bunches suffered residual kick at the rising part of the bump magnetic fields. The maximum oscillation amplitude just after the injection turn corresponds to the angle of 20 μrad, which will hopefully be reduced by further tuning of the fast correction magnet on the basis of the oscillation measurements using the TTPM.

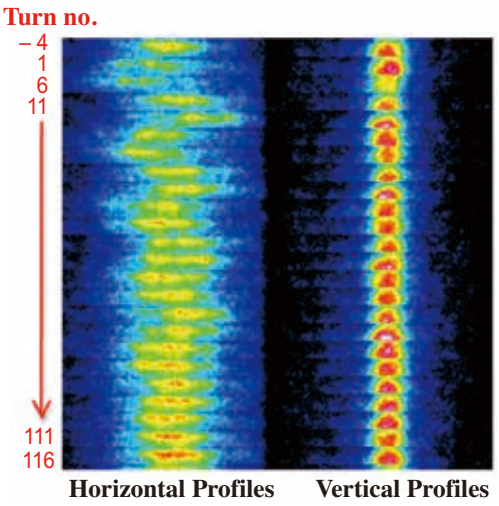

Fig. 8. Example of profiles of photon beam of ID obtained every 5 turns by TTPM. The left and right images are for horizontal and vertical profiles, respectively. The numbers on the left side show the turn numbers after top-up injection of which the turn of the bump orbit excitation is labeled as the zeroth turn (see text).

Development of Compact Fast-Pulsed Power Supply System

We have developed a compact fast-pulsed power supply system to supply the fast kicker magnet system since 2008, with the purposes of generating short-pulsed X-ray in the 1-ps region [7] and suppressing the residual beam oscillation at injection [8].

The location for installation of the kicker magnet had to be selected under the assuming that the existing main accelerator components are left unchanged, and giving the optimum phase advance to maximize the kicker effect. According to the restriction, the space allowed for installation was 30 cm long. To fulfill the required fast rise time with a compact size chassis that fits in the allowed small space, the power supply was divided into two parts: the driving circuit part and the main voltage supply part. The driving part was placed close to the kicker magnet with one turn air coil for reducing the load to the power supply (Fig. 9). In addition to the reduction of the occupied volume, an advantage of separating the power supply by two parts is the easy protection from scattered X-rays of synchrotron radiation because the power supply part

Fig. 9. Setup of power supply system in the accelerator tunnel. The power supply system is placed in the radiation and noise shield box.

is placed outside the accelerator tunnel.

To generate the fast-rise time short pulse with a large output current, a high voltage was supplied to the driving part and switched to the load through Si-MOSFETs (FET). The performance of the power supply largely depends on FET properties, especially the voltage resistance. The voltage resistance increased from 400 V in 2008 to 1200 V as of 2011, and using these 1200-V resistant devices, we have confirmed a 400-ns, 200-A pulsed output with 10-Hz repetition (Fig. 10). We expect the output of 500 A with the output driving module that is now under construction. To increase the output current, FETs were connected in a parallel-series configuration for the output stage. This configuration requires strict synchronization of switching FETs to obtain a short rise time and a large output current without invoking damage overload to the FETs.

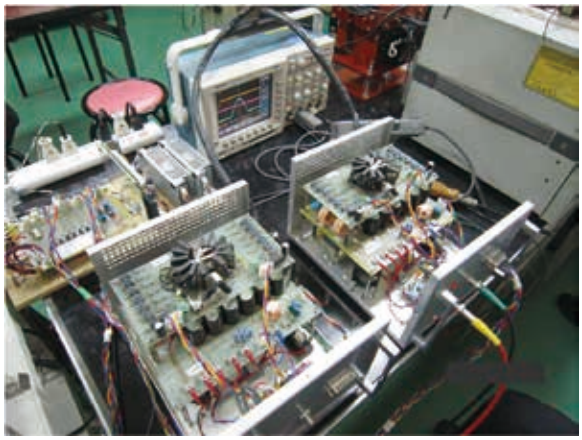

Fig. 10. Photo of improved compact fast-pulsed power supply system using serial-parallel MOSFET connection. With this module, the output of 200 A with a pulse width of 400 ns was achieved in 2012. The case size is 210(W) × 160(H) × 300(D) mm^3.

For practical use, trouble-free operation during user experiment runs is required. However, the power supply failures were caused by the following reasons; 1) high frequency noises caused by the beam wake fields, 2) high voltage induced by the kicked beam on the coil of the kicker magnet, 3) radiation damage from the scattered X-rays, 4) impedance mismatch between the power supply and the coil load that could induce an overvoltage, and 5) FET breakdown with overload caused by the switching of the parallel circuits out of synchronization. To reduce the risk of malfunction, reverse high voltage protection circuits were installed, as well as the radiation and noise shields. With the improvement of the protection circuits and noise and radiation shields, the power supply achieved continuous operation without failure for 40 days.

As the next step, we are planning to improve the power supply by adopting SiC-MOSFET, which has a higher resistance voltage, to reach the 1-kA region in the output current with 200-ns pulse width and 1-kHz repetition.

High Power Test of the Ceramic Window for Sealing WR-1500 Waveguide under Vacuum

We use beam-accelerating cavities resonating at 508.58 MHz in the SPring-8 storage ring and the booster synchrotron. RF input couplers are specific antennae that feed an RF (radio frequency) power into the cavities under vacuum. The power is transmitted from a klystron of RF source to the cavities with a circuit of WR-1500 rectangular waveguides. The coupler transduces the transmission line from the WR-1500 waveguide to a WX-D77 coaxial one terminated with a loop coupling to the cavity. A cylindrical ceramic window was brazed at the coaxial part of the coupler and seals the inside of the cavity in a vacuum. When the window happens to be damaged and leaked, the whole body of the coupler must be replaced with a new one since the brazed window cannot be detached. The replacement procedure is complicated and takes a long time. Therefore, we have developed a compact and replaceable ceramic window bolted to the WR-1500 waveguide to recover from the mechanical failure in a short time.

Figure 11 shows the fabricated window. It is a rectangular plate of low-loss alumina with a purity of 99.8% with a relative permittivity of 9.9 and dimensions of 258.6×80×5 in mm^3. The ceramic was brazed to a rectangular copper frame fitting to the waveguide. The compact body affords us easy

Fig. 11. Fabricated ceramic window for high-power RF input coupler.

assembly in sure vacuum seal and sound RF contact. The window was designed to transmit an RF power of 600 kW CW (continuous wave), which was twice as much as the maximum power in the current cavity operation. The VSWRs of the window were less than 1.1 in a wide frequency range of more than 30 MHz. Figure 12 shows 3D electromagnetic and structural simulations. The maximum electric fields were held down to 0.4 kV/mm in 600 kW operation and smaller than the breakdown limit of 16 kV/mm of the alumina. Two cooling channels with a water flow of 3 *l*/min are arranged on both sides of the ceramic; these channels remove the heat by power loss and reduce the thermal stress in the window to less than the proof stresses of copper and alumina.

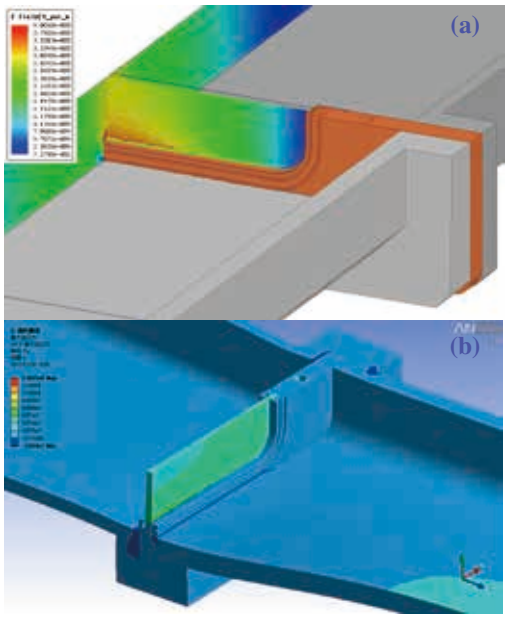

Fig. 12. 3D simulations of **(a)** electric fields and **(b)** stresses in window. The deformation in (b) is depicted exaggeratedly for easy tracing.

We assembled the window and a vacuum waveguide terminated with a short plate and tested it with a standing CW of 150 kW as shown in Fig. 13. The RF and heat loads to the window of the standing wave were almost equivalent to those by a travelling wave of 600 kW. We could successfully and stably transmit the rated RF power without vacuum leakage or damage to the window by RF processing in about 18 h.

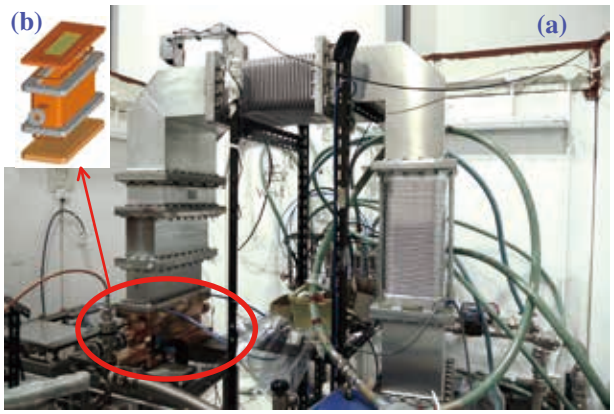

Fig. 13. **(a)** Setup of window for high-power test and **(b)** schematic drawing of window assembly.

Haruo Ohkuma, Shigeki Sasaki

SPring-8/JASRI

*Email: ohkuma@spring8.or.jp

References

[1] T. Tanaka and H. Kitamura: SPECRA code ver. 9.02 (2012).
[2] K. Kobayashi and T. Nakamura: Proc. ICALEPCS 2009, Kobe, Japan, p.659
[3] T. Nakamura: Proc. of IPAC '11, San Sebastian, Spain, p.493
[4] M. Masaki *et al.*: Proc. of IBIC2012, Tsukuba, Japan.
[5] SPring-8 Research Frontiers 2009, p.154.
[6] SPring-8 Research Frontiers 2010, p.152.
[7] C. Mitsuda *et al.*: J. Physics: Conference Series **425** (2013) 042012.
[8] C. Mitsuda *et al.*: Proc. of IPAC'10, Kyoto, Japan, p.2252.